

that produced by the competent substrate. The peaks eluting with 50, 53, and 60% methanol, which represented NCS-chrom spontaneous degradation products, were diminished with the competent substrate. That the new material is the post-activated form of NCS-chrom that is involved in hydrogen atom abstraction from DNA was shown by its incorporation of  $^3\text{H}$  when the substrate was a 16-mer DNA with a  $^3\text{H}$  label at the C-5' of C22 (Fig. 4C). These results show that the conversion of NCS-chrom into a hydrogen-abstracting (presumably radical) species requires the participation of a particular DNA structure and confirm the involvement of C-5' chemistry in the cleavage reaction. Our finding of a new post-activated form of the drug in the presence of bulged DNA contrasts with the thiol-promoted reaction in which the final drug product is the same, whether duplex DNA is present or not (15). Radioactive peaks eluting at 4 min and 30 to 45 min represent cytosine (from the partial spontaneous breakdown of nucleoside 5'-aldehyde) and smaller oligonucleotides, respectively, generated in the DNA damage reaction (Fig. 4C). Quantitation of the three radioactive peaks showed that the amount of  $^3\text{H}$  abstracted by the drug from C-5' is sufficient to account for the DNA products.

DNA cleavage involves general base catalysis and is optimal at pH  $\sim 9.0$ . This observation suggests that drug activation requires ionization of the phenolic hydroxyl group of the NCS-chrom naphthoate moiety, which has an equilibrium constant ( $pK_a$ ) of  $\sim 8.5$  (16). One possibility is that the bent DNA substrate induces a conformational change in NCS-chrom so as to bring the hydroxy naphthoate and the bicyclic enediynes within proximity of the reaction. This change may enhance the ability of a nucleophile, either the phenolate anion or a tautomeric species associated with the naphthoate moiety, to attack C-12 of NCS-chrom and initiate the cycloaromatization reaction to form the radical species (17). It is also possible that this reaction is a spontaneous one (18) and that a subsequent step is modified by the DNA to generate another intermediate form of the drug.

Our study suggests the potential use of NCS-chrom as a general probe for bulged structures in nucleic acids. The resemblance of the structure studied here and that of the trans-activation response sequence in human immunodeficiency-type 1 viral RNA warrants study of the latter as a target for both natural and synthetic enediynes.

## REFERENCES AND NOTES

1. I. H. Goldberg, *Acc. Chem. Res.* **24**, 191 (1991), and references therein.
2. M. D. Lee, G. A. Ellestad, D. B. Borders, *ibid.*, p. 235.
3. Y. Sugiura *et al.*, *Proc. Natl. Acad. Sci. U.S.A.* **86**, 7672 (1989).
4. N. Zein *et al.*, *ibid.* **90**, 2822 (1993).
5. A. G. Myers, *Tetrahedron Lett.* **28**, 4493 (1987).
6. T. Hatayama, I. H. Goldberg, M. Takeshita, A. P. Grollman, *Proc. Natl. Acad. Sci. U.S.A.* **75**, 3603 (1978).
7. L. S. Kappen, C.-q. Chen, I. H. Goldberg, *Biochemistry* **27**, 4331 (1988).
8. A standard reaction (in the dark for 1 hour on ice) contained 50 mM tris-HCl (pH 8.5), 1 mM EDTA, 31-1 DNA that was either 5'  $^{32}\text{P}$ -labeled with [ $\gamma$ - $^{32}\text{P}$ ]adenosine triphosphate and polynucleotide kinase (225  $\mu\text{M}$  phosphate) or 3'  $^{32}\text{P}$ -labeled with [ $\alpha$ - $^{32}\text{P}$ ]cordycepin triphosphate and terminal deoxynucleotidyl transferase (450  $\mu\text{M}$  phosphate), and NCS-chrom (48  $\mu\text{M}$ ). NCS-chrom in methanol was added last (final methanol concentration was  $\leq 10\%$ ). When dsDNA was the substrate, we annealed the  $^{32}\text{P}$ -labeled strand with a 2.5-fold excess of its complementary strand in  $\times 2$  reaction buffer by heating the mixture at  $90^\circ\text{C}$  for 2 min and cooling it slowly. The dried sample was dissolved in 80% formamide for analysis on a 15% sequencing gel. Gel bands were quantitated with a phosphorimager (Molecular Dynamics, Inc., Sunnyvale, CA). About 73% of the starting material was cleaved at T22.
9. L. S. Kappen and I. H. Goldberg, unpublished data.
10. ———, *Biochemistry* **22**, 4872 (1983).
11. J. A. Rice and D. M. Crothers, *ibid.* **28**, 4512 (1989).
12. A. Bhattacharya and D. M. Lilley, *Nucleic Acids Res.* **17**, 6821 (1989).
13. C.-H. Hsieh and J. D. Griffith, *Proc. Natl. Acad. Sci. U.S.A.* **86**, 4833 (1989).
14. DNA was first removed from the reaction mixture (200  $\mu\text{l}$ ) by ethanol precipitation. The supernatant was lyophilized, and the pellet was redissolved in 10% aqueous methanol for analysis by HPLC with a reversed-phase Beckman Ultrasphere octadecylsilane column (5  $\mu\text{m}$ , 4.6 mm by 25 cm). The column was initially eluted for 10 min (1 ml/min) with 10 mM ammonium acetate (pH 5.0), followed by a 60-min linear gradient of 0 to 60% methanol that contained 10 mM ammonium acetate (pH 5.0). Radioactivity in the fractions was quantitated by liquid scintillation counting.
15. D.-H. Chin, C.-h. Zeng, C. E. Costello, I. H. Goldberg, *Biochemistry* **27**, 8106 (1988).
16. M. A. Napier and I. H. Goldberg, *Mol. Pharmacol.* **23**, 500 (1983).
17. Recent  $^1\text{H}$  nuclear magnetic resonance and mass spectroscopic studies of the post-activated drug (O. D. Hensens, D. L. Zink, D.-H. Chin, L. S. Kappen, I. H. Goldberg, unpublished data) indicate that a covalent bond is formed between C-1' and C-12 as a result of the tautomeric generation of an attacking nucleophile at C-1'.
18. After submission of this paper, M. Lamothe and P. L. Fuchs [*J. Am. Chem. Soc.* **115**, 4483 (1993)] reported on model studies that show that  $\alpha$ -hydroxy naphthoate esters can undergo intramolecular alkylation at carbon and both oxygen centers.
19. Supported by U.S. Public Health Service grant CA 44257 from NIH. We thank G. A. Ellestad for calicheamicin  $\gamma_1$  and T. W. Doyle and J. Golik for esperamicin  $A_1$ .

9 June 1993; accepted 28 July 1993

## Rat Annexin V Crystal Structure: Ca $^{2+}$ -Induced Conformational Changes

N. O. Concha,\* J. F. Head, M. A. Kaetzel, J. R. Dedman,  
B. A. Seaton†

Annexins are a family of calcium- and phospholipid-binding proteins implicated in mediating membrane-related processes such as secretion, signal transduction, and ion channel activity. The crystal structure of rat annexin V was solved to 1.9 angstrom resolution by multiple isomorphous replacement. Unlike previously solved annexin V structures, all four domains bound calcium in this structure. Calcium binding in the third domain induced a large relocation of the calcium-binding loop regions, exposing the single tryptophan residue to the solvent. These alterations in annexin V suggest a role for domain 3 in calcium-triggered interaction with phospholipid membranes.

The annexin family of proteins (1) is identified by a characteristic amino acid sequence that contains a highly conserved core region, consisting of four or eight repeats of approximately 70 residues, and a highly variable NH $_2$ -terminal region (2). The conserved core region gives rise to the Ca $^{2+}$ -dependent binding to phospholipid membranes that is shared by all annexins.

N. O. Concha, J. F. Head, B. A. Seaton, Department of Physiology, Boston University School of Medicine, Boston, MA 02118.  
M. A. Kaetzel and J. R. Dedman, Department of Physiology and Biophysics, University of Cincinnati College of Medicine, Cincinnati, OH 45267.

\*Present address: Center for Advanced Research in Biotechnology, University of Maryland, Rockville, MD 20850.

†To whom correspondence should be addressed.

The sequence differences found in the NH $_2$ -terminal regions of the molecules may contribute to the specific cellular function of each annexin.

Amino acid sequence data (3) indicate that annexins do not have the "E-F hand" Ca $^{2+}$  coordinating sites found in calmodulin and its homologs. Several studies suggest that annexins in the absence of membranes have a much lower (millimolar as compared to micromolar dissociation constants) affinity for Ca $^{2+}$  than the E-F hand family; however, when annexins are bound to the phospholipid bilayer, their apparent Ca $^{2+}$ -binding affinity is greatly enhanced (to micromolar levels) (4, 5). The binding of annexins to phospholipids appears to require a membrane or micelle structure,

because soluble phospholipids are bound with very low affinity (5).

Previous annexin V crystal structures (6–8) have identified potential  $\text{Ca}^{2+}$ -binding sites in surface loops on the proposed membrane-facing surface of the molecule (6, 9). Calcium ions have been identified in three of the four homologous domains in annexin V. Each of these domains contains a conserved  $\text{Ca}^{2+}$ -binding motif (Table 1), which is structurally related to the  $\text{Ca}^{2+}$  and phospholipid-binding site of phospholipase  $\text{A}_2$  (6). No  $\text{Ca}^{2+}$  ions have been found in domain 3, where this sequence motif is not conserved (10).

The crystal structure of rat annexin V has been determined to 1.9 Å resolution by multiple isomorphous replacement (Table 2). The amino acid sequences of human and rat annexin V (3) share 92% identity. Most of these substitutions are conservative replacements and occur mainly in domain 1. The two molecular structures are superimposable (Fig. 1) except in domain 3, which differs in conformation despite its close sequence similarity. The rat but not the human annexin V crystal structure shows  $\text{Ca}^{2+}$  bound in this domain, and  $\text{Ca}^{2+}$  ligation is the most likely explanation for the conformational difference (11). Chicken and human annexin V share 78% sequence identity, but their crystal structures show similar conformations and neither has  $\text{Ca}^{2+}$  bound in domain 3 (8).

The conformational difference between the human and rat annexin V crystal structures correlates well with previous spectroscopic results. Fluorescence studies have reported a  $\text{Ca}^{2+}$ -induced solvent exposure of the domain 3 tryptophan in annexin V and, in the presence of phospholipid vesicles, the insertion of this tryptophan into the membrane in close proximity to phospholipid headgroups (12). In the rat annexin V structure, with  $\text{Ca}^{2+}$  bound in domain 3, the tryptophan of the 3AB (13) loop extends away from the molecule (Fig. 2). In contrast, in the crystal structures of annexin V with no  $\text{Ca}^{2+}$  in this domain, the tryptophan is buried in the hydrophobic protein core (14).

**Table 1.** Sequence alignment of the annexin V AB-loop  $\text{Ca}^{2+}$ -binding sites (18). The first three coordination positions (boxed) bind  $\text{Ca}^{2+}$  through carbonyl oxygens. The spatially close but sequentially distant acidic residues occupy the fourth and fifth coordination positions. The remaining two positions may be water molecules.

Domain (residues)	Sequence					
1 (26–31, 72)	M	K	G	L	G	E
2 (98–103, 142)	L	K	G	A	G	D
3 (181–187, 226)	G	E	L	K	W	T
4 (257–262, 301)	M	K	G	A	G	D

In the unligated domain 3 of the human annexin V structure, the carbonyl oxygen of Gly<sup>183</sup> is hydrogen-bonded to the main chain amide group of Lys<sup>186</sup> in a reverse turn. In rat annexin V this interaction is broken, and the corresponding (15) Gly<sup>181</sup> and Lys<sup>184</sup> carbonyl oxygens both bind  $\text{Ca}^{2+}$ . As a result, the lysine side chain adopts a new position pointing in the opposite direction. This repositioning affects the main chain conformation of the adjacent Trp<sup>185</sup>, causing the aromatic side chain to move 18 Å from its original position in the hydrophobic core to the surface location (Fig. 3).

The movement of the tryptophan from a buried to an exposed position would be expected to be energetically unfavorable. However, in the rat annexin V crystal, the tryptophan is stabilized by hydrophobic contacts with an adjacent molecule in the crystal lattice, which may mimic the hydrophobic bilayer environment in membrane-bound annexin. The burying of the tryptophan, as seen in the human annexin V structure, is accompanied by a comparatively strained geometry in the unligated re-

verse turn loop conformation. In the human annexin V structure, Lys<sup>186</sup> and Trp<sup>187</sup> are two of five residues that occur in left-handed helical conformations (6). In the rat annexin V structure, the corresponding residues occur in a more energetically favorable conformation. Thus, the relief of the conformational strain coupled with  $\text{Ca}^{2+}$  binding may provide stabilization energy to the tryptophan-containing loop in its new conformation (16). Membrane binding would further stabilize this conformation. Indirect support for the proposed stability of the 3AB loop is our observation that the crystallographic *b* factors of this region are among the lowest in the molecule, indicating little thermal disorder or flexibility.

Calcium liganding groups in site 3AB of the rat annexin V structure assume the same pentagonal bipyramidal configuration seen in AB sites in the other domains, despite the sequence differences (Table 1). However, the main chain conformation has a slight bend to accommodate the single-residue insertion.

The 3DE loop also binds  $\text{Ca}^{2+}$  in the rat annexin V structure, although  $\text{Ca}^{2+}$  coor-

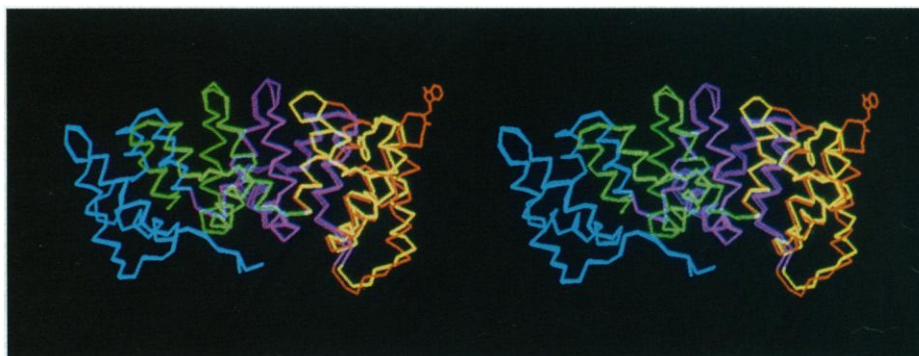


**Fig. 1.** Superposition of  $\alpha$  carbon-backbones of rat and human (6) annexin V molecules. Domain 1, blue, both proteins; domain 2, magenta, both proteins; domain 3, red, rat annexin V; yellow, human annexin V; and domain 4, green, both proteins. Trp<sup>185</sup> (rat) and Trp<sup>187</sup> (human) are also shown.

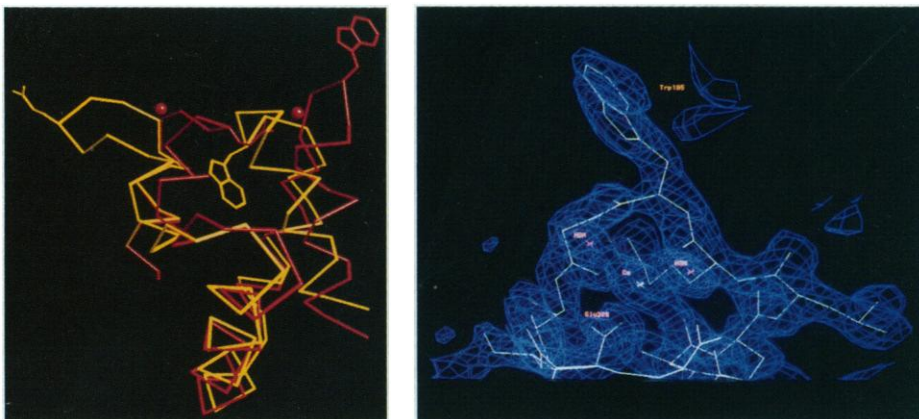


**Fig. 2 (left).** Comparison of 3AB and 3DE loop positions in the  $\text{Ca}^{2+}$ -bound (rat, red) and unligated (human, yellow) states. The  $\text{Ca}^{2+}$  ion on the right is in the AB loop and the  $\text{Ca}^{2+}$  ion on the left is in the DE loop. Prepared with MOLSCRIPT (19). **Fig. 3 (right).** View of the 1.9 Å electron density of the 3AB loop (20).

dination is somewhat different from that in the 3AB site. The 3DE Ca<sup>2+</sup>-binding site includes two peptide carbonyl oxygens (Asp<sup>224</sup> and Thr<sup>227</sup>) and a bidentate carboxylate group (Glu<sup>232</sup>). Consistent with the observation that Asp<sup>224</sup> and Thr<sup>227</sup> provide main chain carbonyl rather than side chain oxygen ligands, neither residue is highly conserved among annexin sequences (6). The existence of this type of site could not be predicted from sequence data. Glutamate-232, which provides an acidic side chain, is invariant in annexins except in the case of domain 7 of annexin VI, where the corresponding residue is basic. However, the residue immediately after is an aspartate, so this domain may include an insertion in the DE loop relative to other such domains.

Comparison of the rat and human annexin V crystal structures reveals even greater displacements in atom positions in the 3DE loop than in the 3AB loop. The carboxylate oxygens of Glu<sup>226</sup> move 23 Å, swinging over the entire DE loop and permitting the Ca<sup>2+</sup> to bind in the 3AB site. Binding of Ca<sup>2+</sup> at the DE site does not appear to trigger this transition, because other DE loops in the molecule can adopt a similar conformation without binding Ca<sup>2+</sup>. The pattern of events implied by these observations is that Ca<sup>2+</sup> binds first to

the 3AB site, triggering movement of the AB loop, which in turn triggers the movement of the 3DE loop into a conformation favorable for binding the second Ca<sup>2+</sup>.

The conformational change that occurs as Ca<sup>2+</sup> is bound in the 3DE loop can be roughly described as a coil-to-helix transition. The biggest changes in backbone angles occur in residues 222 through 224, which adopt characteristic  $\alpha$  helix geometry (17). This positions the Glu<sup>226</sup> side chain so that it can coordinate the Ca<sup>2+</sup> in the adjacent 3AB loop.

In the Ca<sup>2+</sup>-bound form, the AB and DE loops are held together further by a hydrogen bond between the peptide carbonyl oxygen of Glu<sup>226</sup> in the DE loop and the hydroxyl group of Thr<sup>187</sup> in the AB loop. In annexin V, this threonine occurs in the X-K-G-X-G-T (18) sequence in the conserved loop motif and in the W-G-T of the third domain loop. To underscore the importance of this interaction in all annexins, the residue at the position equivalent to Glu<sup>226</sup> in all domains is acidic, and the equivalent to Thr<sup>187</sup> is a hydroxyl-containing residue. In the only exceptions, domain 1 of annexins I and II, the absence of the acidic residue correlates with the absence of the hydroxyl.

Changes in domain 3 appear to facilitate interactions between the adjacent Ca<sup>2+</sup>-

binding loops and also between the loops and the phospholipid membrane. The disposition of hydrophobic residues in the AB loops in general may be an important link between Ca<sup>2+</sup> binding and membrane interaction. In each of the three conserved X-K-G-X-G-T loops, the first hydrophobic (X) residue (Met<sup>26</sup>, Leu<sup>98</sup>, or Met<sup>257</sup>) coordinates Ca<sup>2+</sup> through peptide carbonyl oxygens. These side chains are buried in the protein core, thus helping to anchor the loop. The second hydrophobic residue X (Leu<sup>29</sup>, Ala<sup>101</sup>, or Ala<sup>260</sup>) is solvent-exposed in the Ca<sup>2+</sup>-bound AB conformation, where it may be capable of inserting into the lipid bilayer of the membrane. In domain 3, Leu<sup>183</sup> and Trp<sup>185</sup> both adopt a similarly exposed orientation in the Ca<sup>2+</sup>-bound loop conformation, though neither is directly involved in Ca<sup>2+</sup> coordination. The distribution of the exposed hydrophobic residues across the membrane-facing side of the molecule may explain the strong preference of annexins for membranes and micelles rather than phospholipid monomers.

REFERENCES AND NOTES

1. R. D. Burgoyne and M. J. Geisow, *Cell Calcium* 10, 1 (1989); M. J. Crumpton and J. R. Dedman, *Nature* 345, 212 (1990); C. B. Klee, *Biochemistry* 27, 6645 (1988); C. E. Creutz, *Science* 258, 924 (1992); M. A. Swairjo and B. A. Seaton, *Annu. Rev. Biophys. Biomol. Struct.*, in press.
2. M. J. Geisow, U. Fritsche, J. M. Hexham, B. Dash, T. Johnson, *Nature* 320, 636 (1986); M. J. Geisow, *FEBS Lett.* 203, 99 (1986).
3. R. B. Pepinsky *et al.*, *J. Biol. Chem.* 263, 10799 (1988).
4. P. J. Shadle, V. Gerke, K. Weber, *ibid.* 260, 16354 (1985); D. D. Schlaepfer, T. Mehlman, W. H. Burgess, H. T. Haigler, *Proc. Natl. Acad. Sci. U.S.A.* 84, 6078 (1987); H. T. Haigler, D. D. Schlaepfer, W. H. Burgess, *J. Biol. Chem.* 262, 6921 (1987); M. D. Bazzi and G. L. Nelsestuen, *Biochemistry* 30, 971 (1991).
5. J. F. Tait, D. Gibson, K. Fujikawa, *J. Biol. Chem.* 264, 7944 (1989).
6. R. Huber, J. Römisch, E.-P. Paques, *EMBO J.* 9, 3867 (1990); R. Huber, M. Schneider, I. Mayr, J. Römisch, E.-P. Paques, *FEBS Lett.* 275, 15 (1990); R. Huber *et al.*, *J. Mol. Biol.* 223, 683 (1992).
7. A. Lewit-Bentley, S. Morera, R. Huber, G. Bodo, *Eur. J. Biochem.* 210, 73 (1992).
8. M. C. Bewley, C. M. Boustead, J. Walker, D. A. Waller, R. Huber, *Biochemistry* 32, 3923 (1993).
9. G. Mosser, C. Ravanat, J.-M. Freyssinet, A. Brisson, *J. Mol. Biol.* 217, 241 (1991).
10. In the annexin I crystal structure [X. Weng *et al.*, *Protein Sci.* 2, 448 (1993)], domain 3 contains a Ca<sup>2+</sup> in the AB loop, although the DE loop remains unoccupied. The AB loop assumes the rat annexin V conformation in domain 3. However, almost half of the 3AB loop residues, including Trp<sup>185</sup>, differ from annexin V.
11. The rat annexin V crystals were grown at a final Ca<sup>2+</sup> concentration (20 mM) that was the highest of the published structures. In the "high Ca<sup>2+</sup>" human annexin V structure, crystals were grown at lower Ca<sup>2+</sup> concentration and transferred into solutions containing 50 mM Ca<sup>2+</sup>, where they cracked and annealed (6). In this procedure, the crystal lattice contacts were formed before the transfer to high Ca<sup>2+</sup>, which appears to produce a different result from the cocrystallization procedure. In the rat annexin V crystals, Trp<sup>185</sup> partici-

**Table 2.** Structure determination. Rat annexin V was purified and crystallized as previously described (21). The R3 crystals have unit cell dimensions of  $a = b = 156.9$  Å and  $c = 37.03$  Å. Native diffraction data were collected to 1.87 Å from two crystals on a Xenotronics area detector using CuK $\alpha$  radiation, and derivative data sets were collected to the resolution shown from one crystal each. Data were processed with the XENGEN data processing software (22). Both isomorphous and anomalous difference data from three derivatives were used. Complete details of the structure determination will be published elsewhere (23). The model was built on a Silicon Graphics Iris 4D35 workstation using the software package O (24) and refined using the program XPLOR (25). The final model was refined against  $F\alpha(F) \geq 2$  (where  $\alpha$  is the standard deviation) data from 6 to 1.9 Å resolution. The final 1.9 Å resolution model containing 2528 non-hydrogen atoms had an  $R$  factor (26) of 20.2%, with a bond length root-mean-square deviation (rmsd) of 0.015 Å and a bond angle rmsd of 2.9°. The overall  $b$  factors were 29 and 33 for main chain and side chain atoms, respectively. The last five residues at the COOH-terminus were too disordered to be included in the model. Seven calcium atoms, two sulfate ions, and 40 water molecules were refined. OMIT maps were used to check the Ca<sup>2+</sup>-binding loops and other regions.

Parameters	Native	CMNP*	K <sub>2</sub> PtI <sub>6</sub>	GdCl <sub>3</sub>
Data resolution (Å)	1.87	3.10	2.50	3.05
Data completeness (%)	78.7	88.8	92.0	91.7
Observations (number)	42509	9778	22208	10866
Unique reflections (number)	22374	5661	10709	6078
$R_{\text{sym}}^{\dagger}$	0.0415	0.0376	0.0445	0.0663
Mean fractional isomorphous difference $^{\ddagger}$		0.165	0.216	0.233
$R_{\text{merge}}^{\S}$		0.148	0.173	0.200
Sites (number)		2	3	2
Phasing power $\parallel$		2.35	1.95	1.43

\*CMNP, 2-chloro-4-mercury nitrophenol.  $\dagger R_{\text{sym}} = \sum \sum (|I(h) - \langle I(h) \rangle|) / \sum \sum I(h)$ , where  $I(h)$  is the intensity of the  $i$ th measurement of the reflection  $h$  and  $\langle I(h) \rangle$  is the mean intensity of the  $N$  equivalent reflections. The summation is over all the reflections in a given resolution range.  $\ddagger$ Mean fractional isomorphous difference =  $\sum |F_{\text{PH}} - F_{\text{P}}| / F_{\text{P}}$ , where the summation is over all the reflections in a given resolution range.  $\S R_{\text{merge}} = \sum \sum (|F(h) - \langle F(h) \rangle|) / \sum \sum F(h)$ , where  $F(h)$  is the structure factor amplitude of the  $i$ th measurement of the reflection  $h$ , and  $\langle F(h) \rangle$  is the mean structure factor amplitude of the  $N$  measurements. The summation is over all the reflections.  $\parallel$  Phasing power =  $F_{\text{H}} / E$ , where  $F_{\text{H}}$  is the rms mean heavy atom contribution, and  $E$  is the rms residual defined as  $[\sum (F_{\text{PHC}} - F_{\text{PH}})^2 / N]^{1/2}$  where the summation is over all the reflections in a given resolution range.  $F_{\text{PHC}}$  is the calculated structure factor amplitude of the heavy-atom derivative, and  $F_{\text{PH}}$  is the observed structure factor amplitude of the heavy atom derivative.

- pates directly in lattice contacts, and these crystals dissolve when transferred to low  $\text{Ca}^{2+}$  solutions.
12. P. Meers, *Biochemistry* **29**, 3325 (1990); \_\_\_\_\_ and T. Mealy, *ibid.* **32**, 5411 (1993).
  13. Nomenclature as in (6): AB loops and DE loops separate the antiparallel A and B helices and D and E helices, respectively; numerals identify the domain.
  14. The proposed location of the exposed tryptophan at the polar-apolar interface of the phospholipid bilayer is consistent with tryptophan distribution in other membrane proteins. The partitioning of these side chains at the bilayer surface may promote proper ionic interactions and in gramicidin appears to play a role in ion conductance [W. Hu, K.-C. Lei, T. A. Cross, *Biochemistry* **32**, 7035 (1993)].
  15. Identical residues in domain 3 are numbered two higher in the human annexin V sequence on account of additional residues.
  16. The  $\phi, \psi$  angles of Lys<sup>184</sup> and Trp<sup>185</sup> as observed in human and rat annexin V structures (rat annexin V numbering) are as follows. Lys<sup>184</sup>:  $\phi = 27^\circ$ ,  $\psi = 60^\circ$  (human),  $\phi = -97^\circ$ ,  $\psi = 130^\circ$  (rat); Trp<sup>185</sup>:  $\phi = 31^\circ$ ,  $\psi = 58^\circ$  (human),  $\phi = -77^\circ$ ,  $\psi = 118^\circ$  (rat).
  17. The  $\phi, \psi$  angles for residues 222 to 224 in human and rat annexin V structures (rat annexin V numbering) are as follows. Residue 222:  $\phi = -85^\circ$ ,  $\psi = 8^\circ$  (human),  $\phi = -58^\circ$ ,  $\psi = -43^\circ$  (rat); residue 223,  $\phi = -131^\circ$ ,  $\psi = 147^\circ$  (human),  $\phi = -61^\circ$ ,  $\psi = -41^\circ$  (rat); residue 224,  $\phi = -117^\circ$ ,  $\psi = 135^\circ$  (human),  $\phi = -68^\circ$ ,  $\psi = -40^\circ$  (rat).
  18. Single-letter abbreviations for the amino acid residues are as follows: A, Ala; C, Cys; D, Asp; E, Glu; F, Phe; G, Gly; H, His; I, Ile; K, Lys; L, Leu; M, Met; N, Asn; P, Pro; Q, Gln; R, Arg; S, Ser; T, Thr; V, Val; W, Trp; and Y, Tyr.
  19. P. J. Kraulis, *J. Appl. Crystallogr.* **24**, 946 (1991).
  20. Map coefficients are  $2|F_o| - |F_c|$ , contoured at 1.8 $\sigma$ .
  21. B. A. Seaton, J. F. Head, M. A. Kaetzel, J. R. Dedman, *J. Biol. Chem.* **265**, 4567 (1990).
  22. A. J. Howard, C. Nielsen, N. H. Xuong, *Methods Enzymol.* **114**, 452 (1985).
  23. N. O. Concha, J. F. Head, M. A. Kaetzel, J. R. Dedman, B. A. Seaton, in preparation.
  24. T. A. Jones, S. W. Cowan, M. Kjeldgaard, *Acta Crystallogr. Sect. A* **47**, 110 (1991).
  25. A. T. Brunger, A. Krukowski, J. W. Erickson, *ibid.* **46**, 585 (1990).
  26.  $R$  factor =  $\sum |F_{\text{obs}}(h) - F_{\text{calc}}(h)| / \sum F_{\text{obs}}(h)$ , where  $F_{\text{obs}}(h)$  and  $F_{\text{calc}}(h)$  are the observed structure factor amplitude, and the structure factor amplitude calculated from the model, respectively.
  27. We thank E. and M. Westbrook for assistance with data collection at Argonne National Labs and G. Petsko for advice and for his crystallographic programs. We thank our colleagues in our laboratories, P. Meers for discussion, and K. Allen for help with figures. Supported by National Institutes of Health grants R29-GM-44554 (B.A.S.), RO1-NS-20357 (J.F.H.), and RO1-DK-41740 (J.R.D.); the American Heart Association, Massachusetts Division, Research Grant-in-Aid 13-539-878 (B.A.S.); and an American Cancer Society Junior Faculty Research Award (B.A.S.). Coordinates have been deposited in the Brookhaven Protein Databank (accession number 1RAN).

9 June 1993; accepted 19 July 1993

## Cooperative Interactions Between the *Caenorhabditis elegans* Homeoproteins UNC-86 and MEC-3

Ding Xue, Yuan Tu, Martin Chalfie\*

The POU-type homeodomain protein UNC-86 and the LIM-type homeodomain protein MEC-3, which specify neuronal cell fate in the nematode *Caenorhabditis elegans*, bind cooperatively as a heterodimer to the *mec-3* promoter. Heterodimer formation increases DNA binding stability and, therefore, increases DNA binding specificity. The *in vivo* significance of this heterodimer formation in neuronal differentiation is suggested by (i) a loss-of-function *mec-3* mutation whose product *in vitro* binds DNA well but forms heterodimers with UNC-86 poorly and (ii) a *mec-3* mutation with wild-type function whose product binds DNA poorly but forms heterodimers well.

The differentiation of six touch receptor neurons in the nematode *C. elegans* requires two homeobox genes, *unc-86* and *mec-3*. The *unc-86* gene encodes a POU-type homeoprotein required in touch cell precursors to generate the touch receptor neurons (1, 2). The *mec-3* gene, which encodes a LIM-type homeoprotein, is needed to specify the touch cell fate once the cells have been produced (3–5). The presence of *unc-86* protein (UNC-86) in the touch cells (2), the binding of UNC-86 to the *mec-3* promoter, and the requirement for some of the UNC-86 binding sites *in vivo* for *mec-3*

expression (6) suggest that *unc-86* directly initiates *mec-3* expression. Furthermore, mutation of one UNC-86 binding site in the *mec-3* promoter reveals that *unc-86* is also required to maintain *mec-3* expression (6), a role consistent with the finding that UNC-86 is present in the touch cells throughout the life of the animals (2).

The *mec-3* gene is required for proper expression of genes such as *mec-4* and *mec-7* (3, 7, 8) that are needed for touch receptor function (4, 9), and it is required for the maintenance of its own expression (5, 6, 10). Because *mec-3* protein (MEC-3) binds to its own promoter and mutations in some MEC-3 binding sites affect the maintained expression of *mec-3lacZ* fusions, such autoregulation is likely to be direct (6).

The proteins UNC-86 and MEC-3 bind to overlapping regions in the *mec-3* promoter (Fig. 1A), two of which (CS2 and CS3) are needed for *mec-3* expression (6). We examined the binding of UNC-86 and MEC-3 to oligonucleotides of these regions in gel mobility-shift assays (11). UNC-86 bound differently to the two oligonucleotides, yielding one retarded band with CS2 and two retarded bands with CS3 (Fig. 1B). The two CS3 bands represent the binding of UNC-86 as a monomer and a dimer (12). Homodimer formation has been observed with three other POU-type homeoproteins, Pit-1, Oct-2, and Cfl-1 (13, 14).

As for MEC-3, it bound to both oligonucleotides and resulted in a single retarded species (Fig. 1B), although the binding of MEC-3 to CS2 was weak. When both MEC-3 and UNC-86 were added to each of the oligonucleotides, the MEC-3 band was reduced and a more intense band (the UM complex) appeared at a position near the UNC-86 monomer band. The UM complex contains both MEC-3 and UNC-86 because it can be supershifted by either an antibody to MEC-3 (anti-MEC-3) or an antibody to an influenza virus epitope tag added to UNC-86. In the UM complex, MEC-3 bound at least 24 times as much oligonucleotide (CS2 or CS3) as it did without UNC-86. The binding of oligonucleotide by UNC-86 in the UM complex increased at least sixfold over the binding of DNA to UNC-86 alone. These data suggest that the binding of both proteins to DNA, especially the binding of MEC-3 to DNA, is greatly increased by a cooperative protein interaction. Although the UM complex is observed in gel shifts with both oligonucleotides, most of the following experiments were done with the CS3 oligonucleotide.

Interactions between UNC-86 and MEC-3 were also detected by chemical cross-linking (15) (Fig. 2A), which showed that a heterodimer is formed, and by immunoprecipitation (16) (Fig. 2B), which showed that the proteins can interact without DNA.

Truncated UNC-86 and MEC-3 allow for visualization of the heterodimers in gel shifts and help define the domains needed for these interactions (Fig. 3). The POU domain of UNC-86 [UNC-86(POU)] is sufficient for both DNA binding and heterodimer formation. For MEC-3, a region of only 76 amino acids (amino acids 217 to 293) containing the homeodomain and the adjacent COOH-terminal 16 amino acids was sufficient for DNA binding and heterodimer formation, whereas the MEC-3 homeodomain (amino acids 217 to 277) alone bound DNA but formed heterodimers with UNC-86 on DNA very poorly. The LIM domains, which neither bind DNA nor form heterodimers, appear to inhibit DNA binding. The extrahomeodomain re-

Department of Biological Sciences, Columbia University, New York, NY 10027.

\*To whom correspondence should be addressed.